Published in final edited form as:
Magn Reson Med. 2011 June ; 65(6): 1630–1637. doi:10.1002/mrm.22752.

Improvements in Multislice Parallel Imaging Using Radial CAIPIRINHA

Stephen R. Yutzy[1,2,3], **Nicole Seiberlich**[2], **Jeffrey L. Duerk**[1,2], and **Mark A. Griswold**[2]

[1] Department of Biomedical Engineering, Case Western Reserve University, Cleveland, OH, USA

[2] Case Center for Imaging Research, Department of Radiology, University Hospitals of Cleveland and Case Western Reserve University, Cleveland, OH, USA

[3] Department of Radiology, University of Pittsburgh, Pittsburgh, PA, USA

Abstract

Multislice parallel imaging involves the simultaneous sampling of multiple parallel slices which are subsequently separated using parallel imaging reconstruction. The CAIPIRINHA technique improves this reconstruction by manipulating the phase of the RF excitation pulses to shift the aliasing pattern such that there is less aliasing energy to be reconstructed. In this work, it is shown that combining the phase manipulation used in CAIPIRINHA with a non-Cartesian (radial) sampling scheme further decreases the aliasing energy for the parallel imaging algorithm to reconstruct, thereby further increasing the degree to which a multi-channel receiver array can be utilized for parallel imaging acceleration. In radial CAIPIRINHA, individual bands (slices) in a multislice excitation are modulated with view-dependent phase, causing a destructive interference of entire slices. This destructive interference leads to a reduction in aliasing compared to the coherent shifts one observes when using this same technique with a Cartesian trajectory. Recovery of each individual slice is possible because the applied phase pattern is known, and a conjugate-gradient reconstruction algorithm minimizes the contributions from other slices. Results are presented with a standard 12-channel head coil with acceleration factors up to 14, where radial CAIPIRINHA produces an improved reconstruction when compared to Cartesian CAIPIRINHA.

Keywords

Parallel imaging; multi-slice; radial; CAIPIRINHA

Introduction

A typical MRI examination includes the acquisition of multiple parallel slices to achieve sufficient coverage of the anatomical region of interest. In fact, all MRI techniques use some form of volumetric excitation to excite the spins in the region of interest, typically via one of three approaches: 1) “conventional” 2D slice selection excites sequential versions of individual slices; 2) 3D imaging excites a large slab and uses secondary phase encoding in the slice direction to spatially encode the signal; and 3) multiband imaging simultaneously excites multiple slices using specialized RF pulses designed to excite multiple frequency bands. 3D and multiband excitation techniques offer an SNR advantage over conventional slice selection due to their larger excited volumes, assuming all other factors remain constant.

Corresponding Author Mark A. Griswold Department of Radiology CCIR-MRI University Hospitals of Cleveland Bolwell B124 11100 Euclid Avenue Cleveland, OH 44106 Phone: (216) 844-8085 Fax: (216) 844-8062 mark.griswold@case.edu.

A great deal of previous research has introduced methods in which the signal from multiple simultaneously acquired slices is separated, including the use of extremely large receiver bandwidths (and therefore readout length) (1), RF phase manipulation techniques (2-3), and wavelet encoding (4-5), but they have inherent disadvantages such as severely degraded image quality (1), increased scan time proportional to the number of excited slices (2-3), or inflexible slice selection options to fit a wavelet basis function (4-5). More recently, parallel imaging techniques (6-7) have accelerated image acquisitions with 2D slice selection (8), 3D partition encoding (9), and even non-rectilinear gradient encoding (10-11). The goal of this work is to combine the acceleration capabilities of parallel imaging with RF phase manipulation to achieve higher acceleration factors in a multislice imaging experiment.

Background

Signal localization in MRI is typically accomplished through the use of spatially varying magnetic fields (gradients) to encode the frequency and phase of the signal. Parallel imaging is made up of a family of techniques that accelerates the acquisition by replacing some gradient encoding with encoding based on the spatially differing sensitivity of multiple receiver channels. All parallel imaging techniques suffer from an SNR decrease relative to their fully sampled equivalents, as described in Eq. 1.

$$SNR_{PI} = \frac{SNR_{full}}{g\sqrt{R}} \quad [1]$$

The two sources of decreased SNR are the acceleration factor R, which expresses the theoretical SNR loss from sampling R-times less data, and the “geometry factor” g. The first source of SNR loss in a parallel imaging acquisition can be mitigated by using a volumetric excitation technique such as multiband excitation (8) but the g-factor loss should also be minimized for optimal imaging results. The g-factor is a measure of how well pixels that are aliased due to the specific undersampling pattern can be separated by the characteristics of the receiver array. In other words, g is a pixel-by-pixel measure which describes the effects of the number of receiver channels, their spatial sensitivity variation, noise correlations, and the aliasing pattern of the accelerated k-space sampling pattern. For Cartesian acquisitions, a g-factor map can be readily calculated with simple analytical expressions (6,12), but for more complicated sampling patterns the complete encoding matrix is necessary. It is well known that g-factor losses can be reduced if the amount of aliased energy can be reduced (6). In a multislice imaging experiment, we define “aliased energy” as the total energy in voxels containing signal contributions from multiple slices prior to parallel imaging reconstruction.

Of particular importance to multislice imaging is the fact that most parallel receiver arrays have an uneven placement of receiver elements along the three principal axes. Practically, there is often at least one direction in which there is reduced coil sensitivity variation and hence reduced opportunity to capitalize effectively on parallel imaging acceleration. For example, in many body arrays, the long axis of the body along the Z-axis constrains coil placement to approximately the surface of a cylinder, leaving coverage along the Z-axis (the slice encoding direction for transverse slices) to be sub-optimal for parallel imaging acceleration. Less variation in the receiver sensitivities results in higher g-factor losses and degradation of image quality (at equal acceleration), especially for slices that are relatively close together (i.e., closer than the size of a slice encoding direction coil element).

To address this issue, the CAIPIRINHA technique (13) has been used to significantly decrease g-factor losses by employing a unique phase cycling pattern for the individual

bands (slices) in a multiband excitation. Phase cycling shifts each slice in the phase encoding direction according to the Fourier shift theorem. The shift of each slice relative to the others results in fewer locations where multiple slices are contributing signal to the undersampled image, i.e. there is a reduction in the aliasing energy that must be separated by the parallel imaging reconstruction. The combination of less aliased energy to separate and more distinct coil sensitivity profiles results in better images than conventional parallel imaging reconstruction.

However, the improvement seen with CAIPIRINHA is limited by its Cartesian sampling pattern. When applied to a Cartesian trajectory, line-dependent phase cycling causes coherent shifts in the phase encoding direction (Figure 1B). Although the aliasing energy is reduced by shifting some slice signal into the background regions of the others, the coherent nature of the additional slice signal still leaves a large amount of aliasing to reconstruct (Figure 1C).

Work with alternative trajectories, such as stochastic (14) and rosette (15), has shown that the phase accrual due to off-resonance with a crossing trajectory causes destructive interference and loss of signal. We propose to intentionally cause destructive interference and effectively reduce the previously coherent signal from an entire slice to incoherent background signal using line-dependent phase cycling, as in CAIPIRINHA, in combination with a crossing trajectory such as a radial trajectory, as shown in Figure 1F. We hypothesize that destructive interference in aliased slices will reduce the amount of aliasing energy and consequently improve the quality of the parallel imaging reconstruction.

Theory

In a simultaneous multislice imaging experiment, the sampled k-space data can be represented as the sum of all excited slices, as given in Eq. 2.

$$s = \sum_{a=1}^{SLICES} s_a \qquad [2]$$

In the case of a CAIPIRINHA type experiment, each slice is also modulated by line-dependent phase (Eq. 3), where the phase term Φ_a is the diagonal matrix given in Eq. 4. In Eq. 3, S_a represents the signal from slice a and has rows equal to the number of phase encoding lines or radial projections, and columns equal to the number of readout points.

$$s = \sum_{a=1}^{SLICES} \Phi_a s_a \qquad [3]$$

$$\Phi_a = \mathrm{diag}\left(e^{i\phi_a[1\ldots n]}\right) = \begin{pmatrix} e^{i\phi_a[1]} & & 0 \\ & \ddots & \\ 0 & & e^{i\phi_a[n]} \end{pmatrix} \qquad [4]$$

Individual lines are modulated by the phase $\phi_a[m]$ where m is the row index (phase-encode line or radial projection) with limits given in Eq. 4. For simplicity, we will further examine the case where two slices are simultaneously acquired with no phase cycling on slice 1 ($\phi_1[m] = 0$) and a π phase increment on slice 2 ($\phi_2[m] = m\pi$). In this case, the simultaneously acquired k-space signal is given in Eq. 5.

$$s=\Phi_1 s_1+\Phi_2 s_2=I_1+s\Phi_2 s_2 \quad [5]$$

By defining a general reconstruction operator R (FFT for Cartesian data, gridding and FFT for radial data), the reconstruction can be described as in Eq. 6.

$$\rho_1'=R(s)=R(Is_1)+R(\Phi_2 s_2) \quad [6]$$

Note that this reconstruction is denoted ρ_1' (slice 1 estimate), as it is the image where only slice 1 is in phase but is not a pure reconstruction of slice 1 as it also includes the reconstruction of the destructive interference of slice 2. This reconstruction ρ_1' will therefore result in the superposition of the reconstructions of slice 1 (Figure 1E) and slice 2 (Figure 1F), as shown in Figure 1G. As the phase pattern for slice 2 is known *a priori*, its effects can be reversed by multiplying s by the complex conjugate phase pattern, as given in Eq. 7. Reconstruction (Figure 1H) of an estimate of slice 2 will then be a superposition of destructively interfering slice 1 and in-phase slice 2 and is given in Eq. 8.

$$\Phi_2^* s=\Phi_2^*(Is_1+\Phi_2 s_2)=\Phi_2^* Is_1+Is_2 \quad [7]$$

$$\rho_2'=R\left(\Phi_2^* s\right)=R\left(\Phi_2^* Is_1\right)+R(Is_2) \quad [8]$$

Using the principles shown in the previous example, the general form for reconstruction of any slice estimate ρ_a' is given in Eq. 9, where b is the slice estimate index and a is the slice index.

$$\rho_b'=\sum_{a=1}^{SLICES} R\left(\Phi_b^*\Phi_a s_a\right) \quad [9]$$

Using a radial CAIPIRINHA sampling pattern, each slice estimate contains signal from the slice of interest as well as incoherent signal from other simultaneously acquired slices. If the coil sensitivity patterns at both slice locations are known, it should be possible to minimize the contribution of signal from other slices into each final reconstructed slice. In Cartesian CAIPIRINHA this is accomplished with a conventional parallel imaging reconstruction (such as SENSE or GRAPPA) where one coil sensitivity estimate has the same phase encoding direction shift applied as the phase-cycled slice. With a radial acquisition the final reconstruction requires a more sophisticated conjugate gradient (CG) reconstruction algorithm, described below.

Methods

For the purposes of reporting acceleration factors it is assumed that a “fully sampled” radial acquisition corresponds to the same number of projections as phase encoding lines used in a Nyquist-sampled Cartesian acquisition, rather than what is required by Nyquist for a radial acquisition. True acceleration factors relative to radial Nyquist sampling can be obtained by multiplying the reported acceleration factors by π/2. This convention was chosen so that comparisons between Cartesian and radial acquisitions can be considered constant time comparisons.

Imaging experiments were performed on a 1.5T clinical scanner (Siemens Espree, Siemens Healthcare, Erlangen Germany). A standard gradient recalled echo (GRE) pulse sequence was modified to perform multiband excitation and readout with either a Cartesian or radial trajectory. A vendor-supplied 12 channel head array coil (2 rings of 6 elements each) was used for signal reception. For the radial sequence variant, gradient delay errors were compensated using the simple correction method proposed by Peters et al. (16). For this preliminary work, coil sensitivity maps were acquired separately at each slice location using the same sequence with conventional 2D slice selection. Coil sensitivity maps were masked to represent the object support, and the same maps were used for both techniques. A phantom with sufficient slice direction variation was selected and images were acquired using both Cartesian and radial CAIPIRINHA with the same imaging parameters: (TR/TE/α = 7.5 ms/3.8 ms/45°, 2 slices, 256^2 matrix, 256 PE lines/radial projections, 5 mm slices spaced 50mm apart). *In vivo* imaging was performed on asymptomatic volunteers with the same setup used in the phantom experiments, with slightly different imaging parameters: (TR/TE/α = 11.5 ms/6.0 ms/25°, 2 slices, 256^2 matrix, 256 PE lines/radial projections, 5 mm slices spaced 50mm apart). Written informed consent was obtained in accordance with local IRB.

As described above, estimates of the two slices can be recovered by reconstructing the raw data and the raw data modulated by the conjugate phase pattern. These reconstructions will show some additional signal in the form of shifted versions of the phase cycled slices (Cartesian, Figure 1C-D) or incoherent background signal (radial, Figure 1G-H). To recover the true slices, an iterative reconstruction is employed based on the CG SENSE technique (10) and is shown in Figure 2. The algorithm is initialized using the raw multi-channel data. For each iteration of the reconstruction algorithm, 5 steps are performed: 1) multiplication by coil maps and inverse gridding to k-space, 2) combination of raw data for all slices with their phase patterns into one summed data set, 3) reconstruction of each slice estimate by multiplying by complex conjugate coil map and complex conjugate phase pattern, 4) combination of individual channels by simple summation, and 5) either calculation of difference factors to apply in the next iteration or termination of the algorithm. The approximations shown in Figure 1C-D,G-H can be obtained by pausing the algorithm after the complex sum in the first iteration. The major differences between this algorithm and the original CG-SENSE algorithm are the addition of parallel pathways for each slice, and the additional phase terms in the middle of Figure 2. Since the algorithm is a reconstruction process (shown in the left half of Figure 2) and a sampling process (shown in the right half of Figure 2) repeated within a CG loop, it is necessary to include the small incoherent contributions from other slices in the minimization, hence the phase terms. The relative change from the initial estimate is calculated at each iteration; the algorithm is terminated if the change drops below a pre-determined threshold (10^{-5} for this work) or if the relative change increases for more than one iteration, in which case the previous best result is returned. An additional “maximum iterations” check is also performed, but was not needed in this work. Gridding and inverse gridding are performed using the NUFFT (17) algorithm provided by Jeffrey Fessler's reconstruction toolbox (http://www.eecs.umich.edu/~fessler/). The Cartesian acquisition was also reconstructed using this CG algorithm for comparison purposes, although it also could have been reconstructed with a conventional SENSE algorithm.

Both Cartesian and radial data sets were retrospectively undersampled to in-plane acceleration factors of 1 (i.e. no in-plane acceleration), 3 and 5, corresponding to total acceleration factors of 2, 6 and 10 since two slices were excited in each case. An additional undersampling factor of 14 was used with the *in vivo* data. These factors were chosen because even acceleration factors (i.e. 2, 4, 6) would effectively remove the π phase cycling increment, thus negating the benefits of either the Cartesian or radial CAIPIRINHA. For the

Cartesian data, the undersampling pattern was chosen in such a way as to ensure that the central k-space line was always included. Artifact power was calculated for the phantom experiments using Eq. 10 by comparing each undersampled reconstruction to the fully sampled single slice images that were also used to create coil sensitivity estimates. Both slices were used in the artifact power calculation, although only one is shown in Figure 3.

$$AP = \frac{\sum_{i=1}^{voxels} \left(|\rho_i| - |\rho_{\mathrm{ref},i}| \right)^2}{\sum_{i=1}^{voxels} |\rho_{\mathrm{ref},i}|^2} \quad [10]$$

Results

Phantom results are shown in Figure 3 for total acceleration factors of 2, 6, and 10. Fully sampled single slice images using both trajectories are also shown for comparison. At the minimum acceleration factor, $R_{TOTAL}=2$, both Cartesian and radial images give excellent image quality and minimal additional visible noise. At a higher acceleration factor, $R_{TOTAL}=6$, the radial reconstruction again gives a highly accurate reconstruction with some additional noise. However, the Cartesian image no longer can completely unalias the images, resulting in some residual ghosting. At the highest acceleration factor in this study, $R_{TOTAL}=10$, the Cartesian acquisition exhibits further image quality degradation and no longer represents the object, while the radial acquisition is still accurate, although with further increased noise.

These observations are quantitatively compared to artifact power calculations shown in Figure 4 for both acquisitions and for total acceleration factors of 2, 6, and 10. Fully sampled single slice images (Figure 3A,E) were used as a reference for artifact power calculations. At the lowest simulated acceleration factor ($R_{TOTAL}=2$) both techniques have low and nearly identical artifact powers. At higher acceleration ($R_{TOTAL}=6$) both techniques increase in artifact power, with the Cartesian increasing more than the radial. At the highest acceleration studied ($R_{TOTAL}=10$), the radial acquisition exhibits another slight increase in artifact power, while the Cartesian increases dramatically.

In vivo imaging results are shown in Figure 5 for total acceleration factors of 2 (B, G), 6 (C, H), 10 (D, I), and 14 (E, J). Fully sampled single slice images using both trajectories are also shown for comparison (A, F). At low acceleration factors ($R_{TOTAL}=2$), both Cartesian and radial CAIPIRINHA give high quality and accurate reconstructions, with minimal artifacts or additional noise. As the acceleration factor increases, the Cartesian images show expected increases in noise at $R_{TOTAL}=6$ and become completely unusable at $R_{TOTAL}=10$. The radial images show increases in appearance of noise with acceleration factor, but continues to accurately represent the anatomy all the way up to $R_{TOTAL}=14$.

To determine why the radial results remain viable up to an acceleration factor greater than the number of receiver channels, we studied the effect that undersampling has on Cartesian and radial k-space trajectories. Figure 6 shows the relative amount of k-space energy at each acceleration factor in an R=14 undersampled acquisition. As expected, the Cartesian trajectory has 100% of the energy in k-space at the full R=14 acceleration factors. The radial trajectory spreads the energy of k-space over multiple acceleration factors, with the bulk at lower acceleration factors and only a small portion “seeing” the full R=14 acceleration.

Discussion

We have presented radial CAIPIRINHA as a means to reduce aliasing energy and therefore improve the quality of a parallel imaging reconstruction. Phantom images were retrospectively undersampled and compared qualitatively and quantitatively through artifact power calculations. Two slices were simultaneously acquired using both radial and Cartesian trajectories, with one of the slices excited with a phase increment of π radians between adjacent lines/projections. We found that for low acceleration ($R_{TOTAL}=2$), both Cartesian and radial acquisitions give visually excellent results and low artifact power. As the acceleration factor increases ($R_{TOTAL}=6$) both techniques become visually noisier, but the Cartesian technique cannot completely unalias the images. It should be noted that an acceleration factor of 6 is typically considered to be extremely high acceleration with the vendor-supplied 12-channel head coil used for these experiments. At the highest acceleration factor in this study ($R_{TOTAL}=10$) the radial acquisition again maintains the morphology of the object, albeit with additional noise, while the Cartesian reconstruction fails and the images become primarily artifact with little discernable structure. These trends are confirmed by the artifact power calculations shown in Figure 4, which show slight increases in artifact power for the radial acquisition and severe increases in artifact power for the Cartesian acquisition as acceleration increases. Comparing the artifact power calculations to the image results shows that the radial artifact power increases are largely due to increased appearance of noise, while the Cartesian artifact power increases are largely due to incomplete unaliasing.

The observations in phantom studies are mirrored in the *in vivo* results presented in Figure 5. In this case, results are presented up to R=14, where the Cartesian acquisition shows severe aliasing artifacts while the radial acquisition shows increased noise but still gives an accurate depiction of the underlying anatomy.

These results show both qualitatively and quantitatively that combining the RF phase manipulation of CAIPIRINHA with a radial sampling scheme allows for higher acceleration factors before the appearance of limiting artifacts. In addition, the volumetric nature of the sampling in this technique can offset some of the SNR penalty due to acceleration, although quantifying the SNR benefits are out of the scope for this work.

One reason for the potential gain in performance has to do with the amount of k-space energy that is actually sampled in each trajectory, as shown in Figure 6. In a Cartesian trajectory, it is clear that all areas of k-space share the same level of undersampling, thus resulting in a large fraction of the k-space energy near the center being lost. However, these central regions are fully sampled in a radial trajectory. Even outside of the central region, the effective acceleration is reduced compared to a Cartesian acquisition for all regions except for the outer regions which contain only a small fraction of the total energy. Radial acquisitions can be thought of having their k-space energy spread over multiple acceleration factors, and more heavily concentrated at lower accelerations. Thus especially for high accelerations, it may be that radial trajectories offer a distinct advantage when using parallel imaging that may more than mitigate the increased reconstruction complexity.

For real-time experiments where it is necessary for reconstruction time to not exceed the acquisition time, it may be undesirable to perform an iterative reconstruction. In these cases, a reasonable (although noisier) image (Figure 1G-H) can be obtained very rapidly from a single pass through the reconstruction portion (left half of Figure 2) of the CG reconstruction. The noise-like contributions from other incoherent slices is not minimized in these images, but the method will still retain some of the benefits from radial CAIPIRINHA, namely extremely rapid acquisition and temporal synchronization.

As with all SENSE-based techniques, this technique is highly dependent on accurate coil sensitivity estimates for accurate reconstruction. For this preliminary study we used fully sampled reference images to obtain coil sensitivity estimates and for artifact power calculation. In applications where scan time is critical, other faster methods to obtain coil sensitivity estimates could be used as well. It also should be noted that some sequences which already manipulate the RF phase, such as fully balanced SSFP (aka TrueFISP, FIESTA), can interfere with the phase cycling used by CAIPIRINHA. Some work has been done to address this issue (18). Another potential issue with multiband techniques like these is the need for awareness of the impact on specific absorption rate (SAR) with multiband RF pulses. This may limit the utility of CAIPIRINHA (either radial or Cartesian) in applications with large numbers of simultaneous slices, high flip angles, or high main magnetic field strengths. These concerns can be partially mitigated through the use of more sophisticated multiband RF pulse designs (19-20). Finally, as with Cartesian CAIPIRINHA, this method can be extended to more than 2 simultaneously excited slices provided that each uses a unique phase cycling pattern.

In a parallel imaging reconstruction there are two sources of SNR loss: a factor of $\sqrt{R}$ due to reduced data sampling and the g-factor losses due to the characteristics and unaliasing capabilities of the receiver array and the sampling pattern used. As shown in Figure 3 and Figure 5, both radial and Cartesian CAIPIRINHA techniques show expected SNR losses due to reduced data sampling. As the acceleration factor increases, the differences between the two arise from the different g-factor losses of each reconstruction technique. Since the g-factor is a measure of the amount of aliasing energy related to additional information for the reconstruction problem from the receiver array and the receiver array configuration is identical through all imaging experiments, it is reasonable to assume that the differences in g-factor are due to reduced aliasing energy in the radial technique. This is supported by Figure 1 (C-D, G-H), where it is shown that the same phase cycling pattern has vastly different effects on the amount of aliasing energy in the radial and Cartesian reconstructions. At the lowest acceleration factor (R_{TOTAL}=2) the amount of aliasing energy that must be reconstructed with parallel imaging is well within the limits of this coil configuration and undersampling factor. With the same coil configuration and undersampling factor, less aliasing energy should lead to a higher quality reconstruction. This is demonstrated in Figure 3 for R_{TOTAL}=6 and 10 and Figure 5 for R_{TOTAL}=6 to 14 where the radial reconstructions are still morphologically correct while the Cartesian reconstructions exhibit severely increased artifacts. Artifact power calculations given in Figure 4 confirm this trend.

Conclusions

This work demonstrates that given an identical coil configuration and acceleration factor, higher quality reconstructions can be obtained with the radial CAIPIRINHA technique than Cartesian CAIPIRINHA at moderate to high acceleration factors. Previous work (13) has established that Cartesian CAIPIRINHA always gives at least as good of a reconstruction as conventional parallel imaging, so we can conclude that at moderate to high acceleration factors radial CAIPIRINHA will give a higher quality reconstruction than both Cartesian CAIPIRINHA and conventional parallel imaging.

Acknowledgments

The authors gratefully acknowledge research support from the Ohio Third Frontier Project Innovation Incentive Fellowship (SRY), Siemens Healthcare, and National Institutes of Health grants R01-EB-004637 (JLD) and R01-HL-094557 (MAG). The content is solely the responsibility of the authors and does not necessarily represent the official views of the National Institute of Biomedical Imaging and Bioengineering, the National Heart Lung and Blood Institute, or the National Institutes of Health.

References

1. Weaver JB. Simultaneous multislice acquisition of MR images. Magn Reson Med. 1988; 8(3):275–284. [PubMed: 3205156]
2. Souza SP, Szumowski J, Dumoulin CL, Plewes DP, Glover G. SIMA: simultaneous multislice acquisition of MR images by Hadamard-encoded excitation. J Comput Assist Tomogr. 1988; 12(6): 1026–1030. [PubMed: 3183105]
3. Glover GH. Phase-offset multiplanar (POMP) volume imaging: a new technique. J Magn Reson Imaging. 1991; 1(4):457–461. [PubMed: 1790368]
4. Gelman N, Wood ML. Wavelet encoding for improved SNR and retrospective slice thickness adjustment. Magn Reson Med. 1998; 39(3):383–391. [PubMed: 9498594]
5. Gelman N, Wood ML. Wavelet encoding for 3D gradient-echo MR imaging. Magn Reson Med. 1996; 36(4):613–619. [PubMed: 8892215]
6. Pruessmann KP, Weiger M, Scheidegger MB, Boesiger P. SENSE: sensitivity encoding for fast MRI. Magn Reson Med. 1999; 42(5):952–962. [PubMed: 10542355]
7. Griswold MA, Jakob PM, Heidemann RM, Nittka M, Jellus V, Wang J, Kiefer B, Haase A. Generalized autocalibrating partially parallel acquisitions (GRAPPA). Magn Reson Med. 2002; 47(6):1202–1210. [PubMed: 12111967]
8. Larkman DJ, Hajnal JV, Herlihy AH, Coutts GA, Young IR, Ehnholm G. Use of multicoil arrays for separation of signal from multiple slices simultaneously excited. J Magn Reson Imaging. 2001; 13(2):313–317. [PubMed: 11169840]
9. Blaimer M, Breuer FA, Mueller M, Seiberlich N, Ebel D, Heidemann RM, Griswold MA, Jakob PM. 2D-GRAPPA-operator for faster 3D parallel MRI. Magn Reson Med. 2006; 56(6):1359–1364. [PubMed: 17058204]
10. Pruessmann KP, Weiger M, Bornert P, Boesiger P. Advances in sensitivity encoding with arbitrary k-space trajectories. Magn Reson Med. 2001; 46(4):638–651. [PubMed: 11590639]
11. Seiberlich N, Breuer FA, Blaimer M, Barkauskas K, Jakob PM, Griswold MA. Non-Cartesian data reconstruction using GRAPPA operator gridding (GROG). Magn Reson Med. 2007; 58(6):1257–1265. [PubMed: 17969027]
12. Breuer FA, Kannengiesser SA, Blaimer M, Seiberlich N, Jakob PM, Griswold MA. General formulation for quantitative G-factor calculation in GRAPPA reconstructions. Magn Reson Med. 2009; 62(3):739–746. [PubMed: 19585608]
13. Breuer FA, Blaimer M, Heidemann RM, Mueller MF, Griswold MA, Jakob PM. Controlled aliasing in parallel imaging results in higher acceleration (CAIPIRINHA) for multi-slice imaging. Magn Reson Med. 2005; 53(3):684–691. [PubMed: 15723404]
14. Scheffler K, Hennig J. Frequency resolved single-shot MR imaging using stochastic k-space trajectories. Magn Reson Med. 1996; 35(4):569–576. [PubMed: 8992208]
15. Noll DC. Multishot rosette trajectories for spectrally selective MR imaging. Medical Imaging, IEEE Transactions on. 1997; 16(4):372–377.
16. Peters DC, Derbyshire JA, McVeigh ER. Centering the projection reconstruction trajectory: reducing gradient delay errors. Magn Reson Med. 2003; 50(1):1–6. [PubMed: 12815671]
17. Fessler JA, Sutton BP. Nonuniform fast Fourier transforms using min-max interpolation. Signal Processing, IEEE Transactions on. 2003; 51(2):560–574.
18. Stäb, D.; Gutberlet, M.; Breuer, F.; Blaimer, M.; Hahn, D.; Köstler, H. CAIPIRINHA accelerated simultaneous multi-slice TrueFISP real-time imaging. Honolulu, Hawaii: 2009. p. 2659
19. Cunningham CH, Wood ML. Method for improved multiband excitation profiles using the Shinnar-Le Roux transform. Magn Reson Med. 1999; 42(3):577–584. [PubMed: 10467303]
20. Cunningham CH, Wright GA, Wood ML. High-order multiband encoding in the heart. Magn Reson Med. 2002; 48(4):689–698. [PubMed: 12353287]

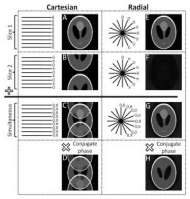

Figure 1.

Schematic of 2 slice Cartesian and radial CAIPIRINHA acquisitions for $R_{SLICE}=2$ and $R_{IN\text{-}PLANE}=1$. Above the solid line, sampling and line-dependent phase patterns are shown for the individual slices. Slice 1 is acquired with no additional phase, and Slice 2 is acquired with a π radian phase increment. The Cartesian acquisition (B) shows the expected FOV/2 shift, while the radial acquisition shows destructive interference (F) in Slice 2. Below the solid line, the results of reconstructing the simultaneously acquired Slice 1 and phase cycled Slice 2 is given. Multiplication by the conjugate phase pattern after acquisition reverses the locations of the Cartesian slices (D) and reverses which of the radial slices is coherent and which is incoherent (H). Note the difference between the coherent aliasing in the Cartesian acquisition (C-D) and incoherent aliasing (G-H) in the radial acquisition.

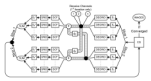

Figure 2.
CAIPIRINHA CG reconstruction diagram
φ - Multiplication by phase cycling pattern
DCF – Multiplication by density compensation function
GRID – Resampling of k-space data to a Cartesian grid
S_γ* - Multiply by complex conjugate of sensitivity of γ^{th} coil
SUM – Complex sum of individual channels
CG – Conjugate gradient method
S_γ – Multiply by complex sensitivity of γ^{th} coil
DEGRID – Resampling of image data to an arbitrary k-space trajectory

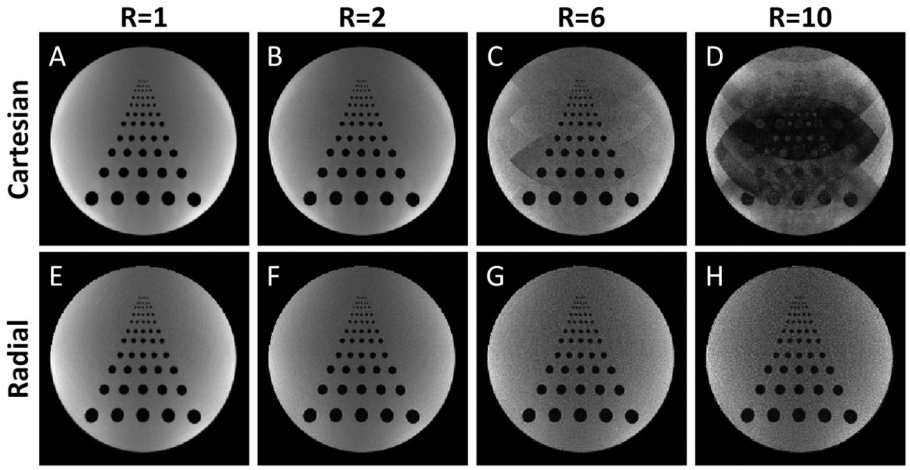

Figure 3.
Cartesian (A-D) and radial (E-H) CAIPIRINHA reconstructions for total acceleration factors of 1 (fully sampled single slice, A,E), 2 (B,F), 6 (C,H) and 10 (D,H). Note that both techniques give high quality and accurate reconstructions at R=2, and as acceleration increases the Cartesian technique can no longer properly reconstruct the slice (C-D) while the radial technique accurately reconstructs the slice with an expected increase in noise. Note that in this experiment two slices were simultaneously acquired; only one is shown for brevity.

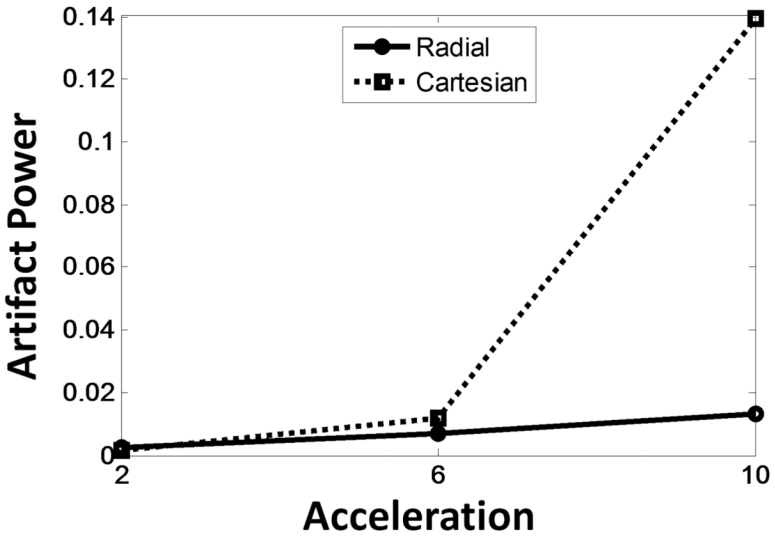

Figure 4.

Artifact power calculations comparing both Cartesian and radial CAIPIRINHA to fully sampled single slice acquisitions of the same trajectory. Both techniques have extremely small artifact power at low acceleration, and increasing artifact power as acceleration increases. Note that the Cartesian technique shows vastly increased artifact power at high acceleration (R=10).

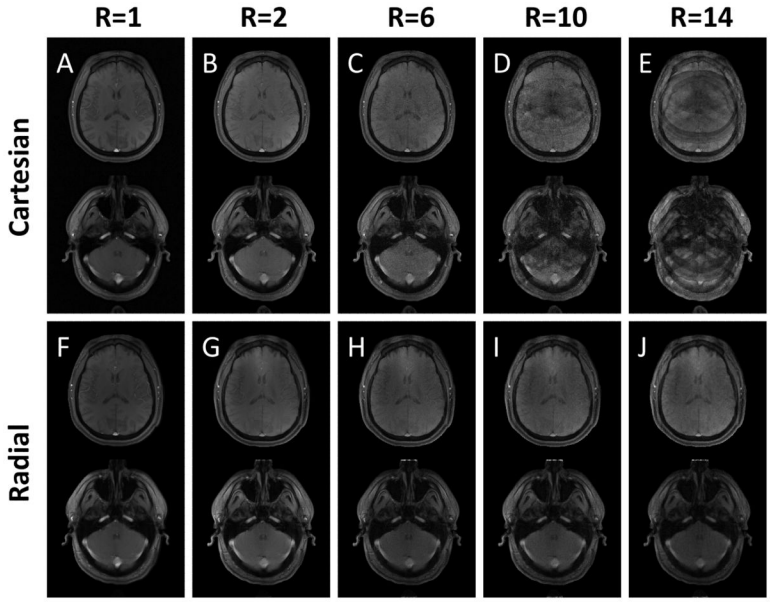

Figure 5.

Cartesian (A-E) and radial (F-J) CAIPIRINHA reconstructions for total acceleration factors of 1 (fully sampled single slice, A, F), 2 (B, G), 6 (C, H), 10 (D, I), and 14 (E, J). R=1 images (A, F) are separately acquired single slice images, while all others are simultaneously acquired with 2 slice CAIPIRINHA. As the acceleration factor increases, the Cartesian acquisition no longer accurately depicts the anatomy at high acceleration (D, E), while the radial acquisition shows an increase appearance of noise but still accurately depicts the anatomy.

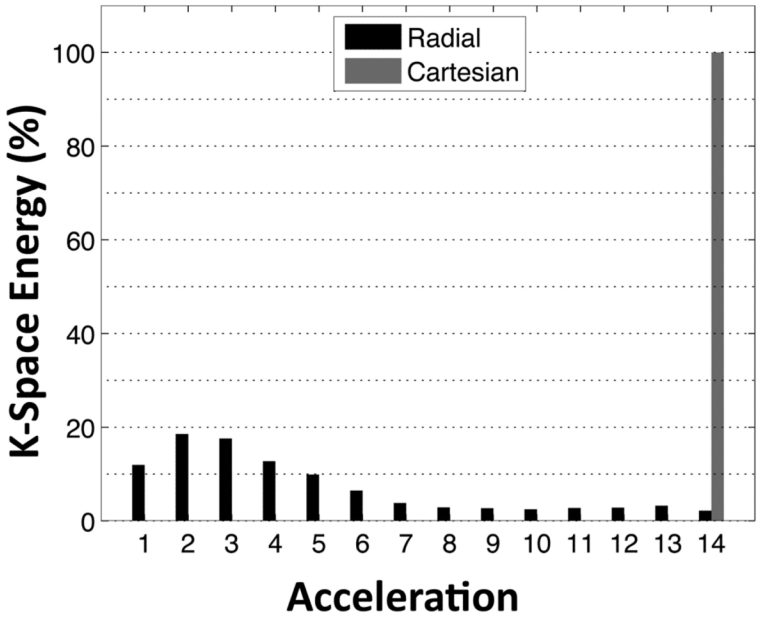

Figure 6.
Relative amount of k-space energy at each acceleration level for an R=14 acquisition. Note that in the Cartesian case 100% of the energy is at the full R=14 acceleration, while in a radial acquisition the bulk of the energy is at lower acceleration levels.